Program Digest, 2019 IEEE International Ultrasonics Symposium (IUS)
Glasgow, Scotland, October 6-9, 2019

Double-profile intersection (DoPIo) elastography: a new approach to quantifying tissue elasticity

Keita A. Yokoyama*[1], Md Murad Hossain[1], Caterina M. Gallippi[1]
[1]Joint Department of Biomedical Engineering
University of North Carolina at Chapel Hill and North Carolina State University
Chapel Hill, NC, USA and Raleigh, NC, USA
*keita@unc.edu

Abstract—Tissue elasticity can be measured by applying an acoustic radiation force (ARF) excitation and tracking mechanical responses like deformation or shear wave propagation via displacement tracking. However, tissue displacements tracked by ultrasound is underestimated due to the shearing of scatterers under the tracking point-spread function. While such displacement underestimation is a source of error in conventional elasticity approaches, we herein present an alternative method that exploits displacement underestimation: double-profile intersection (DoPIo) elastography. We hypothesize that DoPIo can quantify material elasticity in silico.

Index Terms—ARFI, SWEI, elastography, DoPIo

I. Introduction and Background

Traditional methods of ultrasound elastography, such as strain imaging or acoustic radiation force impulse (ARFI) imaging, represent material elasticity qualitatively by depicting displacement responses at a single point in space [1], [2]. In contrast, shear wave methods, like Shear Wave Elasticity Imaging (SWEI), require sampling displacements at multiple positions to evaluate shear wave velocity and find its relation to tissue stiffness [3].

We present Double-Profile Intersection (DoPIo) elastography, a new method of elasticity imaging that hybridizes the two aforementioned approaches. Like ARFI, DoPIo measures displacements in one lateral location to interrogate mechanical property. However, unlike ARFI, each profile is tracked using two different focal configurations, or F-numbers. The two F-numbers result in different tracking beam widths that capture different degrees of scatterer shearing. Larger tracking F-numbers produce laterally wider tracking beams that, for a given ARF excitation, capture a wider range of scatterer shearing [4], [5]. More variability in scatterer shearing results in more displacement underestimation, as does material elasticity; scatterer shearing, thus also displacement underestimation, is resolved faster in stiffer materials than softer ones [4]. Considering these two phenomena in concert, DoPIo deduces elasticity by observing the rate of displacement underestimation resolution under two different tracking F-numbers. Specifically, the intersection time of the displacement profiles generated using the two tracking focal configurations, or the time-intersect (plural: times-intersect), is related to material elasticity through an empirically derived formula.

The feature extraction process would rely on the propagation of shear waves across a PSF, much like spatial sampling methods in SWEI. Thus, we posit that the feature would also exhibit a relationship similar to (1), the process used to infer a SWEI shear modulus estimate μ based on a shear wave speed v_s traveling across a medium with density ρ.

$$v_s = \sqrt{\left(\frac{\mu}{\rho}\right)} \tag{1}$$

The derivation of the empirical formula considered that shear wave velocity relates to the square root of shear elastic modulus, as in (1). This implies an inverse-square relationship between shear elastic modulus and times-intersect. Therefore, an inverse-square relationship was used for our model. Through this approach, we propose DoPIo as a method of elastographic tissue characterization that, while ARFI-like in its reliance on displacement in a single lateral location, allows the quantification of tissue elasticity similarly to SWEI.

II. Methods

A. Ultrasonic Imaging Simulation

Pursuant to methods introduced by Palmeri et al., a digital transducer mimicking the Acuson VF7-3 transducer was defined in Field-II [6]–[8]. Using this transducer object, a 4.21 MHz, 300-cycle ARFI push excitation was simulated with a F/#1.5 focal configuration focused at 25 mm. The beam was scaled to an ISPPA of 7500 W/m^2 at focus, then converted into point loads on an FEM mesh. The mesh spanned 42.0 mm, 20.0 mm, and 12.0 mm in the axial, lateral, and elevational directions, respectively, at an element size of 0.250 mm. The displacement response to the ARFI excitation was simulated using the multiphysics FEM simulator LS-DYNA (LSTC, Livermore, CA, USA) for up to 5 ms after excitation. All preparation for Field-II and post-processing was performed using MATLAB (MathWorks Inc., Natick, MA, USA).

Displacement responses were matched with a field of scatterers with random positions and a Gaussian-distributed echo amplitude. The resulting virtual phantoms were interrogated with a pulse-echo sequence using

Field-II with the aforementioned transducer. Displacements were tracked using a frequency of 6.15 MHz, 10 kHz PRF, and tracking F-numbers of 1.5, 3.0, and 4.5. Displacements were tracked by normalized cross-correlation with a 2-wavelength (500 μm) tracking kernel in an 0.3-wavelength (80 μm) search window [9]. For each push, displacements were tracked at lateral positions spanning from the center of excitation to 6.0 mm laterally on the right side in 0.5 mm increments.

B. Developing the Empirical Model

Once displacements were measured using multiple aperture sizes, a combination of two different F-numbers were chosen, and their displacement profiles were superposed onto each other. For each tracking F-number combinations (tFc), the timestep where the displacement profiles intersected was recorded. These times-intersect were measured for twenty different scatterer realizations in meshes representing ten homogeneous, isotropic, and purely elastic materials with shear elastic moduli ranging from 1 kPa to 37 kPa.

When the times-intersect of a specific tFc, axial depth, and push-track separation distance were determined for all stiffnesses, the times were inverse-squared, and a linear fit model between the times-intersect and shear moduli was generated using a maximum likelihood estimation sample and consensus (MLESAC) method [10]. This fit model generation was repeated for push-track separations up to 6.0 mm, as well as for axial depths ranging between 15.00 mm and 35.00 mm.

C. Performance Evaluation

To evaluate the generated model, the aforementioned methods of tissue excitation, displacement tracking, and intersection detection were repeated in two in silico environments. For both environments, the times-intersect of displacement profiles for F-numbers 1.5 and 4.5 were inverse-squared, passed into the model, and converted into shear modulus estimates.

First, the performance of the model was validated in displacement data for 10 scatterer realizations of 13 homogeneously elastic materials separate from those used to create the original model. The performance of the model was assessed in each additional phantom environment at the focal depth and tracking 2.50 mm away from the region of excitation.

Additionally, measurements were generated for a heterogeneous phantom with a background shear modulus of 10 kPa and a bar with a 5 kPa shear modulus that is infinitely long in elevation and has a square cross-section with side lengths of 2.50 mm. For comparison, multi-track-location SWEI (MTL-SWEI) images were also generated for this dataset, and an identical analysis for inclusion detection was applied.

III. Results

Times-intersect were determined in silico at various spatial positions and shear moduli. For a reference model based off of track F-number combinations of 1.5 and 3.0 based on a scatterer density of 25 per resolution cell, the values were found to be in the distribution depicted in Fig. 1.

Note that Fig. 1 depicts the times-intersect in two different definitions for ”zero”: Fig. 1(a) measures displacement times from the time of the ARFI excitation, thereby incorporating the time of flight for shear wave propagation into intersection detection, whereas Fig. 1(b) bases zero-time from the timepoint in which the later of the two F-numbers’ peak displacements occurred. The latter was intended to standardize the time-intersect to remove the time-of-flight information.

Using a linear relationship derived from the fits in Fig. 1(a), additional shear modulus estimates for homogeneous materials were generated. Results of these simulated images are depicted in Fig. 2, where stiffness estimates largely remained within a 10% boundary of ground truth.

Fig. 3 depicts DoPIo and SWEI images for a heterogeneous digital phantom with a stiffer background shear elasticity, as well as a very long bar with a 2.50 mm square cross-section inclusion with a softer shear modulus.

Employing an ARFI-like image reconstruction method, DoPIo appeared to be capable of illustrating quantitative differences in shear moduli for a heterogeneous, isotropic, purely-elastic phantom with identical scatterer characteristics. A cursory qualitative observation of the DoPIo image reveals an easily identifiable region with clear vertical edges delineating the inclusion from the background. This delineation of inclusion boundaries is more difficult to confirm with the SWEI image, which displays a soft core but a smoother gradient of color that radiates out to the background; this illusion fails to present the soft region as a localized area with heterogeneity in SWEI, unlike DoPIo.

It should be noted that vertically oriented streaks of stiff-appearing regions exist in the edges of the SWEI images. These areas are artifacts from the MTL-SWEI reconstruction method, which involves sequentially tracking the propagation of shear waves across space, only emitting additional ARFI excitations when peak displacements fall below the jitter limit, and stitching together the multiple acquisitions into a single image. As such, the streaks are assumed to be artifacts from the process of image concatenation.

IV. Discussion

The results demonstrate the preliminary capabilities of DoPIo for differentiating shear modulus of elastic materials. Using an FEM-derived empirical model, the intersection of displacement profiles using two known tracking focal configurations for a known axial position

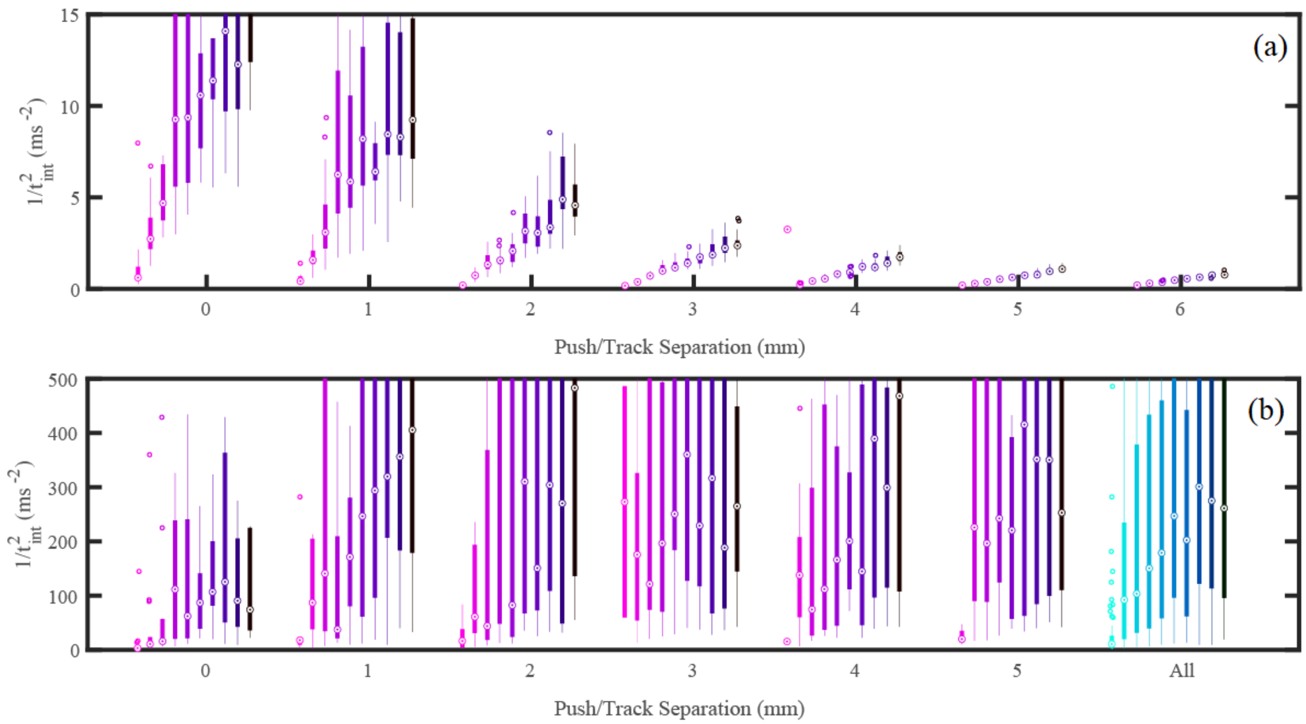

Fig. 1. Distribution of times-intersect at the focal depth for various push-track beam separations. All error bars denote the median, 25th and 75th percentiles, and 95% confidence intervals for times-intersect based on 20 scatterer realizations of F-numbers 1.5 and 3.0. Error bars are color-coded for reference shear moduli from 1 kPa (colored) to 37 kPa (dark) in 4 kPa increments. Subfigure (a) depicts the distribution of times-intersect when they were measured based on the time of ARFI excitation. Subfigure (b) depicts times-intersect distributions with respect to the time to the later of the two peak displacements; the right-most set of whisker plots, in blue, denote all time-intersect distributions without discriminating between push-track separation distances.

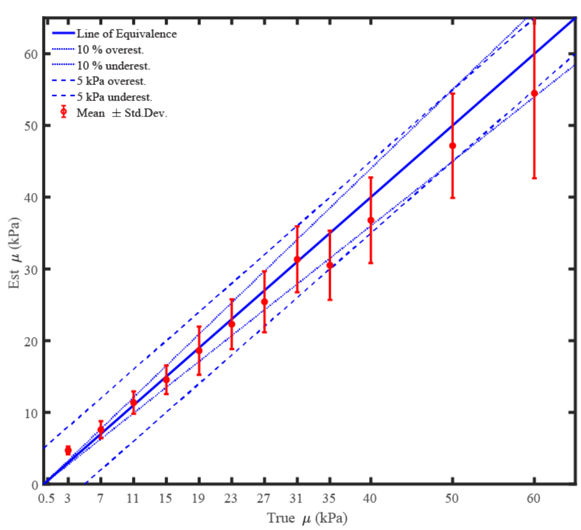

Fig. 2. Shear modulus estimates in homogeneous materials using the derived linear relationship, with track F-numbers of 1.5 and 3.0 being employed at the focal depth of 25.00 mm at 2.50 mm away from the region of ARFI excitation. Stiffness measurements are depicted as the mean and standard deviation of 10 scatterer realizations.

and push-track beam separation distance were converted into shear modulus estimates.

As DoPIo takes advantage of shear wave propagation far away from the ARFI excitation, detecting intersections of displacement profiles are only useful when measurements are not overwhelmed by phenomena like electronic noise, motion artifacts, jitter, and, most importantly, shear wave dispersion and attenuation. As SWEI measurements are equally dependent on robustness against those factors, the useful lateral range for DoPIo is comparable to that of SWEI. However, it is critical to recall that SWEI assumes homogeneity of shear wave velocity measurement over a lateral span of millimeters. While this leads to failure in resolving finer mechanical features in SWEI, DoPIo's pointwise measurements can eliminate the need for spatial sampling, a benefit that may be diagonistically relevant.

The most self-evident limitation to DoPIo is the need for ARFI tracking using more than one F-number. In traditional scanners approved for human clinical use, this requires two sets of independent displacement measurements. If ARF-unrelated tissue translation occurs between acquisitions, measurements may not account for the same spatial positions. This may result in profile intersections at erroneous times, jeopardizing the integrity of a DoPIo estimate. While this effect may be reduced by post-

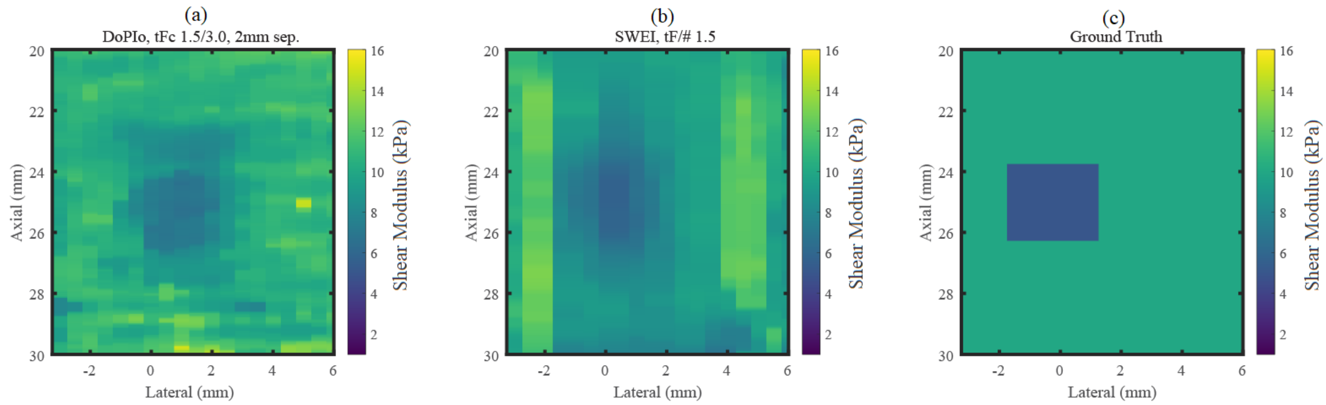

Fig. 3. Median shear modulus estimates for a heterogeneous material with a 10.0 kPa background and a 5.0 kPa square inclusion measuring 2.50 mm for all sides lengths, based on 10 scatterer realizations. Subfigure (a) is the DoPIo image for a track F-number combination of 1.5 and 3.0 in displacements tracked 2.0 mm away from the region of excitation and times-intersect measured from the time of ARF excitation. Subfigure (b) is the SWEI image for a 3.0 mm estimation kernel using a tracking F-number of 1.5, and (c) is the ground truth value that was inputted into the FEM simulation.

processing, a more perfect strategy would rely on only a single tracking ensemble. This approach would involve the acquisition of a single set of channel RF data, then beamforming and displacement-tracking the same dataset using multiple F-numbers simultaneously. We intend to demonstrate a proof-of-concept of such a workflow in vitro with both experimental and clinical scanners.

Another crucial caveat is that the lack of need to sample displacements at multiple locations does not eliminate spatial averaging. While DoPIo measurements are taken at a single position in space, displacement measurements may still be taken at a distance away from the ARFI push position. Depending on the timescale used to define intersections, one may argue that the intersection time is dominated by time-of-flight. While this is true if the timescale is based on the time of ARFI excitation, the measured phenomenon is still a function of changes in the displacement profile due to viscoelastic behavior by tissue under the PSFs. As seen in Fig. 1, while times-intersect were less different between shear moduli regardless of push-track separations without the time-of-flight component, the distributions still appear to suggest some trend. Future work will consider additional models to derive moduli and seek alternate features in the displacement profiles that encode mechanical properties of tissue. The latter direction may employ a machine learning approach so that variability in displacement profiles may not adversely affect stiffness estimates.

V. Conclusion

Through this in silico study, we showed that an empirical model based on the time-intersect can quantify shear elastic moduli in single points of space. We also quantitatively discriminated between soft and stiff regions in a single image using DoPIo with a comparable appearance to SWEI.

Acknowledgment

The authors thank the Siemens Healthineers Ultrasound Division for equipment access and technical support, and UNC Research Computing for supercomputer access. This work was funded by the NHLBI, NINDS, and NIDDK of the National Institute of Health (NIH), under award numbers R01HL092944, R01NS074057, R01DK107740, R43DK112492, K02HL105659, and T32HL069768.

References

[1] J.-L. Gennisson et al, “Ultrasound elastography: principles and techniques,” Diag. and Interv. Imaging. vol. 94, no. 5, pp. 487–495, May 2013.

[2] K. R. Nightingale et al, “Acoustic radiation force impulse imaging: In vivo demonstration of clinical feasibility,” Ultrason. Med. Biol. vol. 28, no. 2, pp. 227–235, Feb. 2002.

[3] A. P. Sarvazyan et al, “Shear wave elasticity imaging: A new ultrasonic technology of medical diagnostics,” Ultrason. Med. Biol. vol. 24, no. 9, pp. 1419–1435, Nov. 1998.

[4] T. J. Czernuszewicz et al, “Experimental validation of displacement underestimation in ARFI ultrasound,” Ultrason. Imaging. vol. 35, no. 3, pp. 196–213, July 2013.

[5] S. A. McAleavey et al, “Estimates of echo correlation and measurement bias in acoustic radiation force impulse imaging,” IEEE Trans. Ultrason. Ferroelectr. Freq. Control, vol. 50, no. 6, pp. 631-641, June 2003.

[6] M. L. Palmeri et al, “Ultrasonic tracking of acoustic radiation force-induced displacements in homogeneous media,” IEEE Trans. Ultrason. Ferroelectr. Freq. Control, vol. 53, no. 7, pp. 1300–1313, Jul. 2006.

[7] J. A. Jensen, “Field: a program for simulating ultrasound systems,” Med. and Biol. Engineering and Computing, vol. 34, pp. 351-353, 1996.

[8] J. A. Jensen and N. B. Svendsen, ”Calculation of pressure fields from arbitrarily shaped, apodized, and excited ultrasound transducers,” IEEE Trans. Ultrason. Ferroelectr. Freq. Control, vol 39, pp. 262-267, 1992.

[9] G. F. Pinton et al, “Rapid tracking of small displacements with ultrasound,” IEEE Trans. Ultrason. Ferroelectr. Freq. Control, vol. 53, no. 6, pp. 1103–1117, 2006.

[10] P. H. S. Torr and A. Zisserman, “MLESAC: a new robust estimator with application to estimating image geometry,” Comp. Vision and Image Understanding, vol. 78, no. 1, pp. 138-156, April 2000.